The $C_4H_6^{\bullet+}$ Potential Energy Surface. 1. The Ring-Opening Reaction of Cyclobutene Radical Cation and Related Rearrangements

G. Narahari Sastry,[†,§] Thomas Bally,*[,†] Vojtech Hrouda,[†,‡] and Petr Cársky*[,‡]

Contribution from the Institute of Physical Chemistry, The University of Fribourg, CH-1700, Fribourg, Switzerland, and J. Heyrovsky Institute of Physical Chemistry, Academy of Sciences of the Czech Republic, Dolejskova 3, 182 23 Prague 8, Czech Republic

Received May 12, 1998

Abstract: Ab initio MO and density functional calculations indicate that the ring opening of the cyclobutene radical cation (**CB**$^{\bullet+}$) follows two competitive pathways, whose energy barriers differ by less than 1 kcal/mol at the highest level of theory employed, RCCSD(T)/cc-pVTZ//UQCISD/6-31G*. The first corresponds to a conrotatory rearrangement to the *cis*-butadiene radical cation (*cis*-**BD**$^{\bullet+}$). The second one leads to *trans*-**BD**$^{\bullet+}$ via a very flat potential energy plateau which comprises cyclopropylcarbinyl-type structures of the type proposed some time ago by Bauld, but the controtatory stereochemistry is preserved also along this process. State correlation diagrams indicate that the rearrangement leading to *trans*-**BD**$^{\bullet+}$ may occur adiabatically along a C_2 reaction coordinate. Despite this, the transition state has no symmetry. This seemingly "unnecessary" loss of symmetry is traced back to the proximity of the ^{2}A and ^{2}B surfaces in the vicinity of the C_2 stationary points, where the two states encounter a strong vibronic interaction which leads to breaking of the C_2 symmetry. These vibronic interactions are also responsible for the general flattening of the potential energy surface in this area.

Introduction

The mechanistic details and the activation barrier for the radical cation analogue of the most fundamental electrocyclic ring-opening reaction, i.e., that of cyclobutene (**CB**) to 1,3-butadiene (**BD**), has been a topic of experimental and theoretical interest for over two decades. Early discussions of this and other pericyclic reactions of radical cations were rooted in Woodward−Hoffmann-type analyses which led to the conclusion that the **CB**$^{\bullet+}$ → *cis*-**BD**$^{\bullet+}$ rearrangement is "forbidden" along concerted con- and disrotatory pathways because both involve crossings of states of different symmetry.[1,2] Nevertheless, as discussed below, the experimental activation barrier for this process is much reduced from the 32.2 kcal/mol prevailing in the neutral.[3] This was ascribed to the fact that the product excited states which correlate with the reactant ground state in both directions lie much lower than in the neutral compounds.[1] The possibility that a complete departure from symmetry, which is required for an adiabatic passage from reactants to products, might lead to a substantial reduction of the activation energy was not considered in these early analyses.

Different experiments have yielded contradictory results for the activation energy of the **CB**$^{\bullet+}$ → **BD**$^{\bullet+}$ ring-opening reaction. An early gas-phase study reported an upper limit of 7 kcal/mol for the parent **CB**$^{\bullet+}$ [4] which was increased to <14 kcal/mol by phenyl or methyl substitution at the double bond, but lowered to <4 kcal/mol by substitution at the CH_2 group [5,6] In contrast, no ring opening of **CB**$^{\bullet+}$ was observed during hours in solid $CFCl_3$ up to 130 K[7] and in CF_3CCl_3 up to 135 K[8] (above these temperatures charge recombination occurs by diffusion). Assuming $t_{1/2} > 1$ h implies $E_a > 10$ kcal/mol (if $\Delta S^{\ddagger} = 0$), i.e., this finding is in contradiction with the above gas-phase estimate for parent **CB**$^{\bullet+}$. Finally, a careful study of 1,2-diphenyltetramethylcyclobutene ionized in solution in a cyclic voltammetry experiment, or by photoinduced electron transfer, led to E_a = 16.5 kcal/mol for this derivative.

Another interesting question in connection with this reaction is whether the conrotatory stereochemistry which prevails in the neutral compounds is preserved in the radical cation. Indeed, Myashi et al. found that *cis*-3,4-diphenylcyclobutene yields exclusively (*E,Z*)-1,4-diphenylbutadiene on photoexcitation of a CT complex or by photoinduced electron transfer.[9] On the basis of the assumption that the butadiene was formed in the cis conformation, where the *E,Z* is less stable than the *E,E* derivative, they concluded that there is a counterthermodynamic driving force for conrotatory ring opening of **CB**$^{\bullet+}$.[9] Unfortunately, these authors did not examine the corresponding *trans*-diphenyl derivative which would have lent more weight to their conclusion. Nevertheless, this finding is in accord with the predictions based on the above-mentioned Woodward−Hoffmann-type deliberations.[2]

The stability of **CB**$^{\bullet+}$ in low-temperature matrices permits the observation of the *photoinduced* ring-opening reaction which

[†] University of Fribourg.
[‡] Academy of Sciences of the Czech Republic.
[§] Present address: Department of Chemistry, Pondicherry University, Pondicherry 605 014, India.

(1) Haselbach, E.; Bally, T.; Lanyiova, Z. *Helv. Chim. Acta* **1979**, *62*, 577−82.
(2) Dunkin, I. R.; Andrews, L. *Tetrahedron* **1985**, *41*, 145.
(3) Cooper, W.; Walters, W. D. *J. Am. Chem. Soc.* **1958**, *80*, 4220.
(4) Gross, M. L.; Russell, D. H. *J. Am. Chem. Soc.* **1979**, *101*, 2082.
(5) Dass, C.; Gross, M. L. *J. Am. Chem. Soc.* **1983**, *105*, 5724.
(6) Dass, C.; Sack, T. M.; Gross, M. L. *J. Am. Chem. Soc.* **1984**, *106*, 5780.
(7) Gerson, F.; Qin, X. Z.; Bally, T.; Aebischer, J. N. *Helv. Chim. Acta* **1988**, *71*, 1069.
(8) Aebischer, J. N.; Bally, T.; Roth, K.; Haselbach, E.; Gerson, F.; Qin, X. Z. *J. Am. Chem. Soc.* **1989**, *111*, 7909.
(9) Miyashi, T.; Wakamatsu, K.; Akiya, T.; Kikuchi, K.; Mukai, T. *J. Am. Chem. Soc.* **1987**, *109*, 5270.

S0002-7863(98)01651-5 CCC: $15.00
Published on Web 08/28/1998

results in spectra that are indistinguishable from those obtained from ionized *trans*-**BD**$^{\bullet+}$.[7] Since *cis*-**BD**$^{\bullet+}$ should be readily distinguishable and since the cis → trans isomerization of **BD**$^{\bullet+}$ is associated with a barrier that cannot be surmounted at low temperature (see section 3.2.4), it was concluded that there must be a direct pathway connecting **CB**$^{\bullet+}$ to *trans*- **BD**$^{\bullet+}$, perhaps on an excited-state surface. This idea was taken up in a recent study by Wiest[10] that appeared when the present paper was in preparation. Wiest showed for the first time that the *ground-state* **CB**$^{\bullet+}$ → *trans*-**BD**$^{\bullet+}$ reaction is *symmetry allowed* along a C_2 coordinate that involves a conrotatory motion of the CH_2 groups.

On pursuing this new reaction mode, Wiest found stationary points at several levels of theory, but—with the exception of the UMP2 level, which lacks credence due to problems with spin contamination—these stationary points turned out to have more than one imaginary frequency, i.e., they did *not* correspond to true transition states. Following the mode perpendicular to the reaction coordinate led to the (unsymmetric) transition state for the conrotatory **CB**$^{\bullet+}$ → *cis*-**BD**$^{\bullet+}$ reaction, which Wiest then explored in detail. He concluded from these results that the symmetry-allowed **CB**$^{\bullet+}$ → *trans*-**BD**$^{\bullet+}$ reaction does not compete with that leading to *cis*-**BD**$^{\bullet+}$.

However, yet another possible reaction mode has to be examined: In 1982, Bauld et al. had argued that the special stability of cyclopropylcarbinyl cations would seem to suggest a pathway involving a corresponding intermediate which they termed (2-cyclopropyl)ylmethyl cation.[11,12] They were indeed able to locate a corresponding stationary point by UHF/STO-3G and MINDO/3, but these levels of theory were not of sufficient reliability to lend strong credibility to this interesting proposal. Thus, Wiest reexamined this possibility at the UMP2/6-31G* level, where he located a very shallow minimum and two transition states showing structural features of a cyclopropylcarbinyl-type radical cation. However, he was unable to confirm this finding by other methods (B3LYP and QCISD), which led him to dismiss this result as an artifact, due to the overestimation of the stability of distonic radical ions by the UMP2 method, and to conclude that the conrotatory reaction leading to *cis*-**BD**$^{\bullet+}$ reaction is the only viable ring-opening mode of **CB**$^{\bullet+}$

Independently, and parallel to Wiest, we undertook it to examine the above possibilities in some detail. Although some of the results we obtained are identical to Wiest's, our study goes considerably beyond his and leads us to fundamentally different conclusions, especially with regard to the role of the **CB**$^{\bullet+}$ → *trans*-**BD**$^{\bullet+}$ reaction and of the intermediate that had been proposed by Bauld. In fact, we will try to show that the **CB**$^{\bullet+}$ ring opening proceeds along *two competing pathways*, both of which retain the conrotatory stereochemistry in the **BD**$^{\bullet+}$ product. One of these paths leads via a very flat region of the potential energy surface which comprises also transition states that connect to another C_4H_6 isomer, bicyclobutane (**BCB**), that had not been considered by Wiest. In fact, we conclude that the ring opening of **CB**$^{\bullet+}$ may be governed by dynamics and is hence not amenable to treatment within the framework of classical transition-state theory.

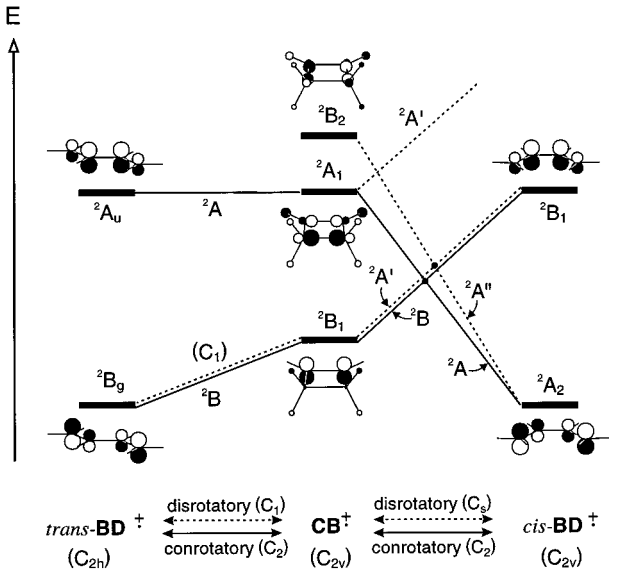

Figure 1. State correlation diagrams for different modes of the **CB**$^{\bullet+}$ → **BD**$^{\bullet+}$ ring-opening reaction. MO pictures designate the singly occupied MO in each state.

In Figure 1 we summarize the possibilities that emerge from a consideration of state symmetries of **CB**$^{\bullet+}$ and **BD**$^{\bullet+}$, including both con- and disrotatory ring-opening modes. In the reaction leading to *cis*-**BD**$^{\bullet+}$, both modes are state symmetry forbidden along C_2 or C_s pathways, respectively, which implies the *necessity* for a departure from symmetry to effect an adiabatic transition from reactant to product. In contrast, this is not required for the conrotatory ring opening to *trans*-**BD**$^{\bullet+}$, whereas the total loss of symmetry along the corresponding disrotatory reaction obviates the need for any such considerations.

After a presentation of the computational methods on which the present study is based, we will examine the different possibilities in sequence and discuss our findings which do not invariably conform with the qualitative expectations based on Figure 1.

Computational Methods

Different computational methods are available to treat radical ions.[13] Ab initio SCF calculations may be done using either a spin-restricted (ROHF) or unrestricted Hartree−Fock (UHF) formalism. The former has the advantage of giving a pure doublet wave function, but it is prone to symmetry breaking and it does not take into account effects of spin polarization. Conversely, UHF calculations, permit to model spin polarization and therefore lead to lower total energies, but this advantage comes at the expense of contamination of UHF wave functions with spin states of higher multiplicities which expresses itself in deviations of the $\langle \mathbf{S}^2 \rangle$ expectation value from the value of 0.75 for pure doublets. Both symmetry breaking and spin contamination can lead to artifacts, especially when one uses perturbative schemes (i.e., the popular MP2 method) for the evaluation of electron correlation. In finite orders, these only work well when the reference SCF wave function is a good approximation to the correlated one, and in the case of open-shell systems, the above-mentioned flaws of ROHF and UHF may constitute serious impediments in this regard, which may lead to pathological behavior.

The more sophisticated, but computationally more expensive coupled cluster (CC)[14] and/or quadratic CI (QCI) methods,[15] which may be regarded as infinite-order perturbative procedures, are less sensitive to

(10) Wiest, O. *J. Am. Chem. Soc.* **1997**, *119*, 5713.

(11) Belville, D. J.; Chelsky, R.; Bauld, N. L. *J. Comput. Chem.* **1982**, *3*, 548.

(12) Note that this is *not* the same as the methylcyclopropane radical cation proposed as an intermediate in the fragmentation of **BD**$^{\bullet+}$ by Russell et al.: Russell, D. H.; Gross, M. L.; Greef, J. v. d.; Nibbering, N. M. M. *J. Am. Chem. Soc.* **1979**, *101*, 2086.

(13) Bally, T.; Borden, W. T. In *Reviews in Computational Chemistry*; Lipkowitz, K. B., Boyd, D. B., Eds.; VCH-Wiley: New York, 1998; Vol. 13, in press.

(14) Bartlett, R. J.; Stanton, J. F. In *Reviews in Computational Chemistry*; Lipkowitz, K. B., Boyd, D. B., Eds.; VCH Publishers: New York, 1994; Vol. 5, p 65.

the choice of the reference wave function, in particular whether it is spin-restricted or unrestricted.[16] Therefore, we have elected to locate all stationary points at the UQCISD/6-31G* level and to use the RCCSD(T) method,[17] coupled with Dunning's polarized triple-ζ (cc-pVTZ) basis set[18] for the evaluation of relative energies. This protocol has been found to lead to "chemical accuracy", i.e., energies within 1 or 2 kcal/mol of the experimental numbers, in many cases. The CC and/or QCI methods often give very similar results when based on restricted or unrestricted wave functions.

In recent years, evidence has been accumulating which shows that methods based on density functional theory (DFT) hold great promise to solve many of the problems mentioned above. In the Kohn−Sham (KS) implementation,[19] DFT attempts to model the exact density via a set of noninteracting electrons described by auxiliary one-electron wave functions (MOs) such as they are used also in HF theory and then to express the effects of exchange and correlation as functionals of that density. This makes KS-DFT calculations in large part isomorphic to HF calculations, but it should be realized that it is now the density and not the wave function that is optimized variationally. This has important consequences with regard to open-shell systems, where the auxiliary wave function is usually chosen to be unrestricted to allow for spin polarization. Nevertheless, DFT wave functions usually show negligible degrees of spin contamination.[20]

In the present work, we used the gradient-corrected exchange functional, of Becke,[21] which, when combined with the correlation functional of Lee, Yang, and Parr (LYP)[22] gives rise to the UBLYP method for open-shell systems. In addition, Beckes three-parameter (B3) and the so-called "half-and-half" (BH&H) exchange functionals[23] were also used in conjunction with the LYP correlation functional to give the UB3LYP or UBH&HLYP methods. The last method proved to be needed for the location of transition states which involve a localization of spin and charge in one part of a molecule, which is often impossible with BLYP or B3LYP due to the incorrect dissociation behavior of these methods for radical ions.[24]

All stationary points were located and characterized by vibrational analyses using both SCF and the three DFT methods, as well as UMP2 and UQCISD, always with the 6-31G* basis set. After noting the great similarity of B3LYP and QCISD structures, the former method was used to establish the connection of saddle points with minima on both sides by intrinsic reaction coordinate (IRC) calculations.[25] The same was done at the UMP2 level in cases where this method gave substantially different transition state structures. The above calculations were done with the Gaussian 94 program package.[26] Finally, RCCSD-(T)/cc-pVTZ single-point calculations (204 basis functions for C_4H_6) were carried out at both the QCISD and the B3LYP geometries with the Molpro program system[27] on a NEC SX-4 vector computer.

We also checked the viability of single-determinant approaches by performing complete active space (CASSCF) calculations with an active space comprising seven electrons in eight active orbitals, on all the stationary points. In all cases, the CASSCF wave function was described to >90% by the reference determinant and no individual excited configuration contributed to more than 4%. An exception to this are the excited states of $\mathbf{BD}^{\bullet+}$ which are poorly described by single configurations,[28] but as these do not play an important role in the present investigation, we refrained from using multideterminantal theory on any larger scale. Furthermore, conical intersections were located with the state-averaged CASSCF method.[29,30] In the reference UHF wave function, the $\langle \mathbf{S^2} \rangle$ values showed significant deviations from 0.75 for *cis*-$\mathbf{BD}^{\bullet+}$ (0.93), *trans*-$\mathbf{BD}^{\bullet+}$(0.91), and $\mathbf{BCB}^{\bullet+}$ (0.81) whereas it was below 0.8 in all other regions of the $C_4H_4^{\bullet+}$ potential energy surface.

3. Results and Discussion

3.1. Structures and Energetics of Reactants and Products. Table 1 gives the relative energies of the stable $C_4H_6^{\bullet+}$ isomers, $\mathbf{CB}^{\bullet+}$, *cis*-$\mathbf{BD}^{\bullet+}$, *trans*-$\mathbf{BD}^{\bullet+}$, and $\mathbf{BCB}^{\bullet+}$ at various levels of theory, whereas the structures with the most important geometry parameters are given in Figure 2. First we note that, with regard to the exothermicity of the $\mathbf{CB}^{\bullet+} \rightarrow \mathbf{BD}^{\bullet+}$ ring-opening reaction, ΔE_{ro}, the UHF and ROHF predictions deviate in the opposite directions from those obtained at the RCCSD(T) level. UHF overestimates ΔE_{ro} by about 5 kcal/mol, whereas ROHF underestimates it by a similar amount. The reason for this is that spin polarization is more important in the conjugated $\mathbf{BD}^{\bullet+}$ than in $\mathbf{CB}^{\bullet+}$. This effect is not accounted for by ROHF, which therefore puts $\mathbf{BD}^{\bullet+}$ at an energetic disadvantage. In contrast, $\mathbf{BD}^{\bullet+}$ is artificially stabilized by the spin contamination which is an inevitable byproduct of the modeling of spin polarization by the UHF method. Also, we note that the ROHF wave functions for $\mathbf{BD}^{\bullet+}$ and $\mathbf{BCB}^{\bullet+}$ suffer from artifactual symmetry breaking, which creates serious problems in numerical computations of derivatives at higher levels.

Going to second-order perturbation theory does not solve the problem: the slow convergence of the UMP series for spin-contaminated wave functions results in an energy disadvantage of $\mathbf{BD}^{\bullet+}$ relative to the less contaminated $\mathbf{CB}^{\bullet+}$ which leads to an underestimation of ΔE_{ro}. Conversely, the general tendency of MP2 to overestimate the correlation energy comes to bear in RMP2 where $\mathbf{BD}^{\bullet+}$ is slightly overstabilized relative to $\mathbf{CB}^{\bullet+}$. Apart from that, RMP2, where no analytical second derivatives are available, is hampered by the symmetry breaking of the ROHF wave function mentioned above. This demonstrates that one must go beyond SCF or MP2 to obtain reliable predictions with regard to the $C_4H_6^{\bullet+}$ potential energy surface which is the target of the present investigation.

However, we note already here that the DFT methods listed in Table 1 give results in reasonable accord with RCCSD(T) at a fraction of the computational cost. In all cases admixture of HF exchange density brings the results closer to the benchmark values. Also noteworthy is the fact, the relative RCCSD(T) energies obtained at the QCISD and at the B3LYP geometries differ by 0.1 kcal/mol or less for all species. This is an indication that B3LYP geometries are reliable, at least at potential energy minima.

Both UHF and ROHF underestimate the stability of the highly strained $\mathbf{BCB}^{\bullet+}$,[31] which is slightly more stable than $\mathbf{CB}^{\bullet+}$ at the reference level, by about 6 and 11 kcal/mol, respectively. Here, second-order perturbation theory works quite well for

(15) Pople, J. A.; Head-Gordon, M.; Raghavachari, K. *J. Chem. Phys.* **1987**, *87*, 3700.
(16) Stanton, J. F. *J. Chem. Phys.* **1994**, *101*, 371.
(17) Knowles, P. J.; Hampel, C.; Werner, H.-J. *J. Chem. Phys.* **1993**, *99*, 5219.
(18) Woon, D. E.; Dunning, T. H. *J. Chem. Phys.* **1993**, *98*, 1358.
(19) Kohn, W.; Sham, L. J. *Phys. Rev.* **1965**, *140*, A1133.
(20) Baker, J.; Scheiner, A.; Andzelm, J. *Chem. Phys. Lett.* **1993**, *216*, 380.
(21) Becke, A. D. *Phys. Rev. A* **1988**, *38*, 3098.
(22) Lee, C.; Yang, W.; Parr, R. G. *Phys. Rev. B* **1988**, *37*, 785.
(23) Becke, A. D. *J. Chem. Phys.* **1992**, *97*, 9173.
(24) Bally, T.; Sastry, G. N. *J. Phys. Chem. A* **1997**, *101*, 7923.
(25) Gonzalez, C.; Schlegel, H. B. *J. Chem. Phys.* **1989**, *90*, 2154.
(26) Frisch, M. J.; Trucks, G. W.; Schlegel, H. B.; Gill, P. M. W.; Johnson, B. G.; Robb, M. A.; Cheeseman, J. R.; Keith, T.; Petersson, G. A.; Montogomery, J. A.; Raghavachari, K.; Al-Laham, M. A.; Zakrzewski, V. G.; Ortiz, J. V.; Foresman, J. B.; Cioslowski, J.; Stefanov, B. B.; Nanayakkara, A.; Challacombe, M.; Peng, C. Y.; Ayala, P. Y.; Chen, W.; Wong, M. W.; Andres, J. L.; Repogle, E. S.; Gomperts, R.; Martin, R. L.; Fox, D. J.; Binkley, J. S.; DeFrees, D. J.; Baker, J.; Stewart, J. P.; Head-Gordon, M.; Gonzales, M. C.; Pople, J. A. *Gaussian 94, Revision B1 and D4*; Gaussian, Inc.: Pittsburgh, PA, 1995.
(27) MOPLRO is a package of ab initio programs written by Werner et al.: Werner, J.-J.; Knowles, P. J.; Almlöf, J.; Amos, R. D.; Deegan, M. J. O.; Elbert, S. T.; Hampel, C.; Meyer, W.; Peterson, K.; Pitzer, R.; Stone, A. J.; Taylor, P. R.; Lindh, R. MOLPRO, Revision 96.1, 1996.
(28) See, for example: Fülscher, M. P.; Matzinger, S.; Bally, T. *Chem. Phys. Lett.* **1995**, *236*, 167.
(29) Ragazos, I. N.; Robb, M. A.; Bernardi, F.; Olivucci, M. *Chem. Phys. Lett.* **1992**, *197*, 217.
(30) Bearpark, M. J.; Robb, M. A.; Schlegel, H. B. *Chem. Phys. Lett.* **1994**, *223*, 269.
(31) Bally, T. *Theochem* **1991**, *73*, 249−264.

Table 1. Energies (kcal/mol) of Stable $C_4H_6^{\bullet+}$ Isomers Relative to the Radical Cation of Cyclobutene (**CB**$^{\bullet+}$) at Different Levels of Theory[a]

method	**CB**$^{\bullet+}$ [b]	*cis*-**BD**$^{\bullet+}$	*trans*-**BD**$^{\bullet+}$	**BCB**$^{\bullet+}$
UHF	−154.610 765	−23.2	−27.2	5.6
ROHF	−154.608 262	−15.1	−18.8	10.6
UMP2	−155.094 519	−14.9	−19.6	−1.9
RMP2	−155.094 770	−21.0	−25.0	−4.6
BLYP	−155.558 310	−22.9	−26.7	2.4
B3LYP	−155.641 728	−21.0	−24.6	2.4
BH&HLYP	−155.541 606	−19.9	−23.7	3.1
UQCISD	−155.123 617	−18.1	−21.1	−0.2
RCCSD(T)// B3LYP[c]	−155.330 589	−18.7 (−17.5)	−22.1 (−21.0)	−0.7 (−0.4)
RCCSD(T)// UQCISD[c]	−155.330 626	−18.6 (−17.9)	−22.1 (−21.4)	−0.8 (−0.7)

[a] All calculations are done with 6-31G* basis set except where indicated. [b] Absolute energies in hartrees for structure optimized at the respective level, except where otherwise indicated. [c] RCCSD(T) single-point calculations with the cc-pVTZ basis set at optimized B3LYP or UQCISD geometries, respectively. The values in parentheses correspond to ΔH_{298} (thermochemical corrections from B3LYP and UQCISD structures and frequencies, respectively).

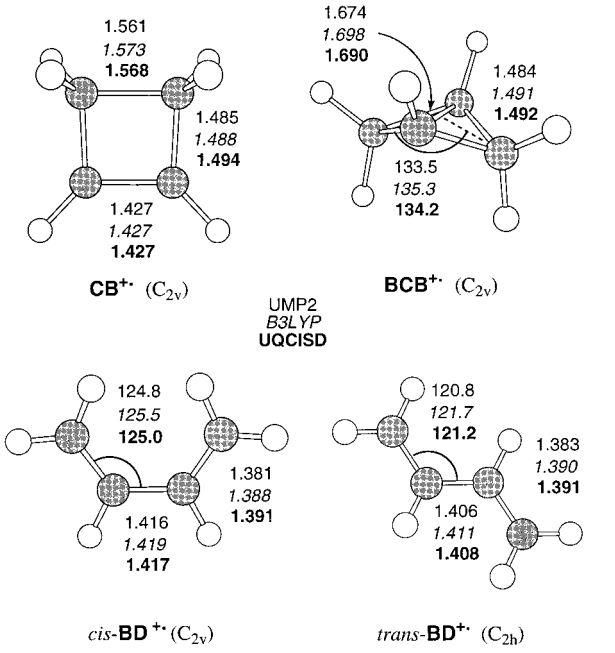

Figure 2. Pertinent geometrical parameters of stable $C_4H_6^{\bullet+}$ isomers obtained by UMP2 (normal), B3LYP (italic), and QCISD (bold), all with the 6-31G* basis set. Full sets of Cartesian coordinates, energies, and thermal corrections are available in the Supporting Information.

correcting the error at the SCF level, but this is in part a lucky coincidence. Also, RMP2 cannot be used for frequency calculations due to the instability of the ROHF wave function for **BCB**$^{\bullet+}$ to symmetry breaking. The DFT methods also put the bicyclic isomer at a disadvantage, but much less so than the HF methods. We had noted a similar tendency in calculations on [1.1.1]propellane and its radical cation.[32] In this case, admixture of HF exchange density does not help to improve the result, on the contrary.

As a consequence of our finding that the restricted MP2 method does not appear to be a practicable alternative for searching the $C_4H_6^{\bullet+}$ potential energy surface, and much less to characterize any stationary points, we refrained from further use of this method in the following work. Before going into a detailed exploration of the energy surface, we present some

(32) Müller, B.; Ingr, M.; Bally, T. To be published.

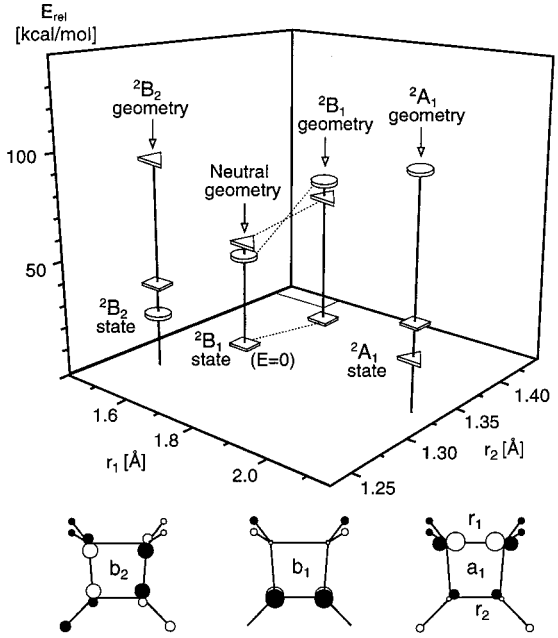

Figure 3. B3LYP/6-31G* energies of the lowest three electronic states of **CB**$^{\bullet+}$ at the respective equilibrium geometries, as well as at the neutral geometry (relative to the energy of the $^2B_1$ ground state at the neutral geometry). Note that each state becomes the ground state at its equilibrium geometry.

results pertaining to the electronic structure of the stable reactants and products.

3.1.2. Electronic Structure of CB$^{\bullet+}$. From Figure 1 it becomes evident that excited states are involved in the correlations of **CB**$^{\bullet+}$ and **BD**$^{\bullet+}$ along symmetry-preserving pathways. Hence, knowledge of the positions and the structures of these excited states is important for understanding the energetics of the rearrangement process. Therefore we offer in Figure 3 a description of these features for the lowest three states of **CB**$^{\bullet+}$, $^2B_1$, $^2A_1$, and $^2B_2$, which arise by ionization from the MOs of the corresponding symmetries depicted at the bottom.

The first feature which becomes evident from this figure is that upon adiabatic relaxation each of these states becomes the respective ground state. The structural changes associated with these relaxations are in line with expectations on the basis of the nodal properties of the MOs: On going from the neutral geometry to that of the most stable ionic state, $^2B_1$ (square), the length r_2 increases due to removal of an electron from the π-bond. In contrast, relaxation of the $^2A_1$ state (triangles) results in a lengthening of the opposite σ_{C-C} bond to over 2 Å due to removal of an electron from the strongly bonding a_2 σ-MO. Finally, as expected, ionization from b_2 (circles) results in a shortening of r_1 and r_2 which is accompanied by a lengthening of the two lateral σ_{C-C} bonds (not shown in the figure).

It should, however, be noted that the stationary points attained by relaxation within C_{2v} symmetry are not minima, except in the case of the most stable $^2B_1$ state which is already the ground state at the neutral geometry. The $^2A_1$ stationary point turns out to be a transition state (**TS0**), whereas the $^2B_2$ stationary point is a second-order saddle point. One interesting consequence of the disposition of states shown in Figure 3 is that it is *not* necessary to leave C_{2v} symmetry to effect a crossover from the reactant $^2B_1$ ground state to the product ground-state surface, and we will see that the lowest points of intersection of the $^2B_1$ with the $^2B_2$ and the $^2A_1$ states do indeed retain C_{2v} symmetry.

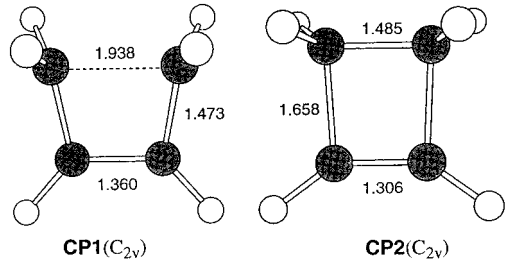

Figure 4. Geometry of the $^2B/^2A$ (**CP1**) and the $^2A'/^2A''$ crossing point (**CP2**) in **CB**$^{\bullet+}$ as obtained by state-averaged CASSCF method.

3.1.3. Electronic Structure of BD$^{\bullet+}$. We and others have noted earlier that excited states of polyene radical ions in general and **BD**$^{\bullet+}$ in particular are not amenable to a correct description by single-determinant methods.[28] Thus, the first excited state of *trans*-**BD**$^{\bullet+}$, which is a minimum at the (3,4)CASSCF level, is found by all single-determinant methods to be a second-order saddle point with substantial negative frequencies ($\nu_i = -481$ and -359 cm^{-1} at B3LYP). By CASSCF, the first excited state of *cis*-**BD**$^{\bullet+}$, in the C_{2h} symmetry of the ground state, is a saddle point ($\nu_I = -110$ cm^{-1}) for interconversion of two slightly more stable gauche forms, but it is again a second-order saddle point by all methods based on single determinants ($\nu_i = -465$ and -333 cm^{-1} at B3LYP).

3.2. Exploration of the $C_4H_6^{\bullet+}$ Potential Energy Surface. All discussions in this section will refer to B3LYP energetics and intrinsic reaction coordinate (IRC) calculations, unless otherwise specified. Excited-state surfaces were generated by single-point B3LYP calculations at the geometries corresponding to selected points along the IRC. The geometries obtained by B3LYP (as well as by BLYP and BH&H) are generally very similar to those at the UQCISD level. The other methods (UHF, ROHF, and UMP2) give significantly different results for some parts of the potential energy surface, in particular in the flat region that we will denote the "Bauld plateau". The most contrasting behavior is encountered at the UMP2 level, and therefore, we will summarize some UMP2 results in a separate section. Full details on the UHF and ROHF results will not be given because the qualitative features found at these levels are not always confirmed by correlated calculations.

3.2.1. CB$^{\bullet+}$ → *cis*-BD$^{\bullet+}$ Reaction. As shown in Figure 1, both the conrotatory (C_2) and the disrotatory paths (C_s) connecting **CB**$^{\bullet+}$ to *cis*-**BD**$^{\bullet+}$ are symmetry forbidden because the respective reactant ground states correlate with product excited states, which leads to state crossings. Therefore we first located the conical intersections for the $^2B/^2A$ state crossing, **CP1**, for the conrotatory path, and for the $^2A'/^2A''$ crossing, **CP2**, for the disrotatory path, using the state-averaged CASSCF method.

As it turns out, both conical intersections correspond to structures of C_{2v} symmetry, a possibility which had already become evident from Figure 3 above and which was thus confirmed. Figure 4 shows that **CP1** distinguishes itself by a very long C−C bond, flanked by weakly pyramidalized CH_2 groups, which indicates a tetramethylene-type species, ready to collapse to *cis*-**BD**$^{\bullet+}$ by twisting the CH_2 groups.

Conversely, **CP2**, which is higher in energy than **CP1** by about 5 kcal/mol, has two long lateral bonds and thus resembles a complex cation poised to dissociation to ethylene and acetylene. It shows no sign of breaking the CH_2-CH_2 bond (in fact, its length has *decreased* from that in **CB**$^{\bullet+}$), from which we conclude that this does not represent the real crossing point leading to the ground-state surface of *cis*-**BD**$^{\bullet+}$. Unfortunately, all attempts to find another $^2A'/^2A''$ conical intersection, corresponding to that for the disrotatory ring opening, invariably converged back to **CP2**. From this we conclude that this crossing must occur at considerably higher energy than **CP1** and that the same applies to the saddle point which would arise through mixing of the two states on departure from C_s symmetry.

Turning to the conrotatory opening motion of **CB**$^{\bullet+}$, Figure 5 (left) describes this process along a C_2 symmetric reaction coordinate. As in the above case of the disrotatory ring opening, the crossing of the reactant (^2A) and product ground-state surfaces (^2B) occurs while the molecule retains C_{2v} symmetry, i.e., before any rotation of the CH_2 groups has occurred. Relaxation of the $^2A_1$ state of **CB**$^{\bullet+}$ leads to a transition state, **TS0**, with a very long CH_2-CH_2 bond (2.07 Å). IRC calculations show that **TS0** connects to the ground state of **CB**$^{\bullet+}$ along both directions of the imaginary normal mode. Thus it acts as a transition state for an automerization of **CB**$^{\bullet+}$ and has no practical significance. Conrotatory twisting of the CH_2 groups within C_2 symmetry, starting from **TS0**, leads to a second-order saddle point **SP2-1**, which lies only 0.3 kcal/mol above **TS0** by B3LYP (at UQCISD, it is isoenergetic, but at RCCSD(T), it lies again about 1 kcal/mol higher). From there, the system collapses freely to the ground state of cis-**BD**$^{\bullet+}$ ($^2A_2$) by further conrotation of the CH_2 groups. At the same time, the ^2B surface (obtained by single-point calculations at some points of the IRC leading from **TS0** via **SP2-1** to *cis*-**BD**$^{\bullet+}$) connects adiabatically to the first excited state, $^2B_1$, of the product.

Of course the system can avoid the $^2A/^2B$ state crossing by loss of symmetry which occurs if one moves in the direction of the imaginary normal mode that is perpendicular to the conrotatory C_2 reaction coordinate at **SP2-1**. Thereby one finds the true transition state, **TS1** for the conrotatory **CB**$^{\bullet+}$ → *cis*-**BD**$^{\bullet+}$ ring-opening reaction, which is depicted above Table 2, where some important geometry parameters are listed. The key feature of this transition state, which had been located previously by Borden[33] and by Wiest,[10] is the strong nonsynchronicity of the two CH_2 group's rotation, as expressed by the difference in the angles ϕ and ω in Table 2. Although this difference, as well as the absolute values of the two angles, varies somewhat between different kinds of calculations, this does not strongly affect the calculated activation enthalpy (see below).

Other noteworthy features of **TS1** are the nonplanarity of the carbon backbone as expressed by the dihedral angle θ and the pronounced disparity of the $CH-CH_2$ bond lengths, that to the nearly perpendicular CH_2 group (r_2) being ca. 0.07 Å longer than that to the other one (r_4). The drawing of the HOMO of **TS1** above the IRC plot on the right side of Figure 5 shows the reason for this: about half of the spin is delocalized in what can be regarded as an allylic moiety, with correspondingly short bond lengths, whereas the other half is localized on the nearly perpendicular CH_2 group, which is not linked by any π-bonding to the rest of the molecule. In fact, this allylic character of the $C_2-C_3-C_4$ moiety is probably responsible for the fact that the C_2-C_3 bond in **TS1** is shorter than in **CB**$^{\bullet+}$ or **BD**$^{\bullet+}$. Most importantly, the IRC calculation (Figure 5, right) shows that the stereochemistry is preserved along the entire reaction path for the conrotatory ring-opening reaction.

The barrier for this process depends quite strongly on the level of theory (cf. Table 3 below). If we take the RCCCSD-(T)/cc-pVTZ//QCISD/6-31G* result as a benchmark ($\Delta E_0 =$ 18 kcal/mol, $\Delta H_0 = 16.8$ kcal/mol), then UHF and ROHF overestimate the barrier by 9 and 12 kcal/mol, respectively. The

(33) Du, P.; Borden, W. T. Personal communication.

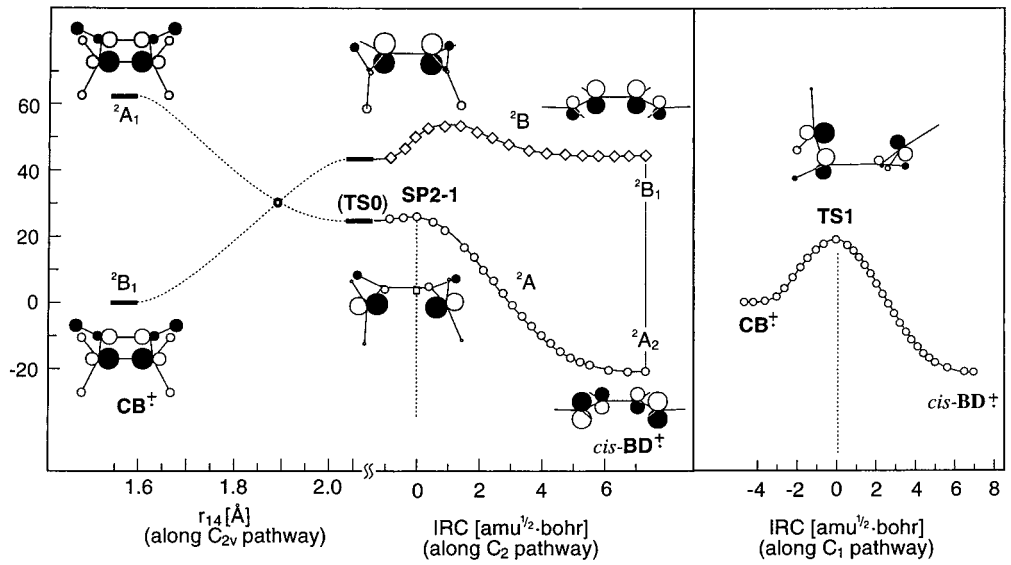

Figure 5. Energy profile for the conrotatory $\mathbf{CB}^{\bullet+} \rightarrow$ *cis*-$\mathbf{BD}^{\bullet+}$ ring-opening reaction from B3LYP/6-31G* IRC calculations. Insets show the singly occupied MO for different states at stationary points on the reaction pathway. Left: reaction profile under maintenance of C_2 symmetry (note that the state crossing occurs in C_{2v} symmetry!). Right: reaction profile with no symmetry restrictions (SOMO at geometry of **TS1**). The excited-state surface is composed of points (squares) vertically above the ground-state IRC points (circles).

Table 2. Key Geometrical Parameters (Bond Lengths in Å and Bond Angles in deg) of the Transition State **TS1** for the Conrotatory $\mathbf{CB}^{\bullet+} \rightarrow$ *cis*-$\mathbf{BD}^{\bullet+}$ Ring-Opening Reaction

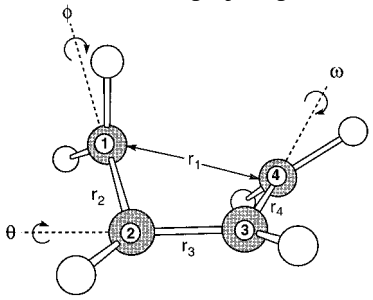

method[a]	r_1	r_2	r_3	r_4	θ^b	ϕ^c	ω^c
UHF	2.115	1.472	1.389	1.402	20.4	69.7	39.4
ROHF	2.221	1.479	1.329	1.448	5.7	81.3	58.8
BLYP	2.211	1.476	1.391	1.423	15.8	73.2	40.7
BH&HLYP	2.154	1.457	1.380	1.397	19.0	68.8	33.5
B3LYP	2.186	1.467	1.385	1.411	17.1	70.8	38.1
UQCISD	2.165	1.467	1.396	1.407	21.1	66.6	35.0

[a] All calculations with the 6-31G* basis set. [b] Dihedral angle $C_1-C_2-C_3-C_4$. [c] Angle of rotation of CH_2 groups; due to the pronounced pyramidalization of these groups, this was defined as the dihedral angle C−C−C−X plus 90°, where X is the midpoint between the two H atoms.

behavior of the DFT models is interesting: whereas the "pure" BLYP model underestimates the barrier by about 3 kcal/mol, the B3LYP prediction is within less than 1 kcal/mol of the benchmark result, while admixture of more HF exchange density, as in the BH&H model, leads again to a clear overestimation by about 5 kcal/mol. Thus, some well-balanced admixture of HF exchange density seems to be beneficial to compensate the tendency of DFT methods to underestimate activation barriers.[34,35]

Finally, we propose a possible reason for our inability to locate a transition state for the disrotatory ring opening of $\mathbf{CB}^{\bullet+}$: If two mechanisms compete along a similar pathway (i.e., if the overlap between the reaction coordinates for the two pathways is significant), it may be impossible to find independent transition-state structures for both processes. In such cases, the search for a saddle point converges invariably to a single transition state which has dominant character of one of the two competing reaction pathways.[36,37] In the present case we note that the con- and the disrotatory processes initially follow a similar reaction coordinate (i.e., lengthening of the C_2-C_3 bond while maintaining C_{2v} symmetry). After that, they will begin to diverge, but since all symmetry must be lost on the way from $\mathbf{CB}^{\bullet+}$ to $\mathbf{BD}^{\bullet+}$, the two mechanisms may mix. In fact, **TS1** does not clearly indicate whether the rotation of the CH_2 groups will eventually be con- or disrotatory because one of them has undergone almost no rotation at the transition state, so it formally carries some character of both processes.

3.2.2. $\mathbf{CB}^{\bullet+} \rightarrow$ *trans*-$\mathbf{BD}^{\bullet+}$ Reaction. The possibility of this ring-opening mode, which is symmetry allowed both along a con- and a disrotatory pathway (cf. Figure 1), was first pointed out by Wiest.[10] His search for a C_2 transition state for this reaction led him to a stationary point which had, however, two or more imaginary modes, except at the UMP2 level where it was a first-order saddle point. At the other levels, the imaginary mode with the less negative frequency was shown to connect $\mathbf{CB}^{\bullet+}$ to *trans*-$\mathbf{BD}^{\bullet+}$ along a conrotatory C_2 reaction pathway. Following the symmetry-breaking imaginary mode which is associated with a larger negative curvature of the potential surface led Wiest to **TS1** discussed above. Thus, no unambiguous evidence for a viable pathway connecting $\mathbf{CB}^{\bullet+}$ directly to *trans*-$\mathbf{BD}^{\bullet+}$ has been provided to date.

Our results on the C_2 conrotatory pathway (B3LYP IRC shown in Figure 6, top panel) confirm Wiest's findings at all levels. However, we should note that single-point calculations along the C_2 IRC on the ^2A state which corresponds to $\pi \rightarrow \pi^*$ excitation of $\mathbf{CB}^{\bullet+}$ show that this state comes rather close to the ground-state ^2B surface in the region of **SP2-2**. This indicates the possibility of vibronic interactions that may be

(34) Johnson, B. G.; Gonzales, C. A.; Gill, P. M. W.; Pople, J. A. *Chem. Phys. Lett.* **1994**, *221*, 100.
(35) Durant, J. L. *Chem. Phys. Lett.* **1996**, *256*, 595.
(36) Reddy, A. C.; Danovich, D.; Ioffe, A.; Shaik, S. *J. Chem. Soc., Perkin Trans. 2* **1995**, 1525.
(37) Sastry, G. N.; Danovich, D.; Shaik, S. *Angew. Chem., Int. Ed. Engl.* **1996**, *35*, 1098.

Table 3. Relative Energies (kcal/mol) of Various Species on the Cyclobutene Ring-Opening Surface

		BLYP[a]		B3LYP[a]		BHANDH[a]		UQCISD[a]		RCCSD(T)[b]//B3LYP		RCCSD(T)[b]//UQCISD	
species	n_{imag}	ΔE_0	ΔH_{298}	ΔE_0	ΔH_{298}	ΔE_0	ΔH_{298}	ΔE_0	ΔH_{298}	ΔE_0	ΔH_{298}	ΔE_0	ΔH_{298}
CB$^{\bullet+}$	0	0.00	0.00	0.00	0.00	0.00	0.00	0.00	0.00	0.00	0.0	0.00	0.0
cis-**BD**$^{\bullet+}$	0	−22.91	−21.53	−20.97	−19.84	−19.89	−19.11	−18.09	−17.36	−18.67	−17.54	−18.64	−17.91
trans-**BD**$^{\bullet+}$	0	−26.55	−25.18	−24.64	−23.53	−23.67	−22.92	−21.79	−21.07	−22.12	−21.01	−22.09	−21.37
BCB$^{\bullet+}$	0	2.48	3.01	2.39	2.75	3.09	3.26	−0.21	0.09	−0.72	−0.36	−0.81	−0.69
TS0	1	22.51	20.83	25.12	23.31	27.80	25.80	25.63	23.61	22.81	21.00	22.63	20.61
TS1	1	15.24	14.58	18.88	17.98	23.12	21.88	21.91	20.72	18.28	17.38	18.00	16.81
TS2	1	—[c]	—[c]	22.18	21.19	23.32	22.47	20.77	20.33	19.18	18.19	18.21	17.77
TS3	1	20.94	20.55	22.08	22.22	23.06	22.24	20.65	20.02	19.00	19.14	18.96	19.33
TS4		43.53	41.95	39.57	37.86	40.60	38.61	39.28	37.53	32.85	31.14	32.90	31.16
TS5	1	—[d]	—[d]	—[d]	—[d]	7.61	6.34	6.29	4.54	—[d]	—[d]	6.27[e]	4.52[e]
SP2-1	2	22.55	20.33	25.41	23.08	28.54	26.00	25.63	26.90	23.82	21.49	23.95	21.49
SP2-2	2	21.39	19.72	25.31	23.52	30.10	28.01	27.80	25.64	23.97	22.18	23.95	21.79
SP2-3	2	42.89	40.38	48.02	45.28	53.87	50.20	50.91	47.99	45.96	43.22	45.51	43.48

[a] All the geometries are fully optimized within the symmetry constraints and verified by frequency calculations using 6-31G* basis set. Full sets of Cartesian coordinates, as well as total energies and thermal corrections are available in the Supporting Information. [b] RCCSD(T) single-point calculations with the cc-pVTZ basis set at the B3LYP/6-31G* or QCISD/6-31G* geometries, respectively. [c] **TS2** could not be located by BLYP. [d] **TS5** could not be located by BLYP and B3LYP. [e] From UCCSD(T)/6-31G* calculations on **CB** and **TS4**. RCCSD(T) could not be performed as MOLPRO has convergence problems at the HF level for **TS4**.

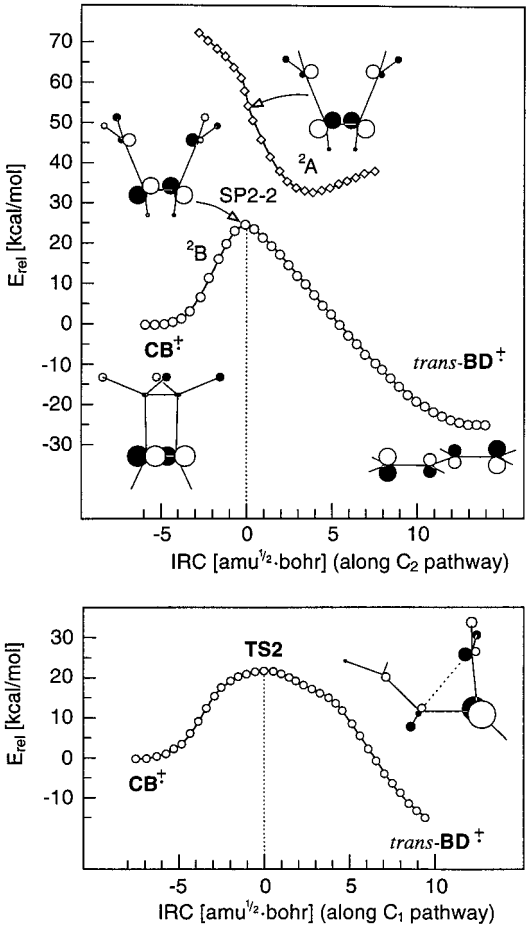

Figure 6. Energy profile for the conrotatory **CB**$^{\bullet+}$ → *trans*-**BD**$^{\bullet+}$ ring-opening reaction from B3LYP/6-31G* IRC calculations. Insets show the singly occupied MO for different states at stationary points on the reaction pathway. Top: reaction profile under maintenance of C_2 symmetry. The excited-state surface is composed of points (squares) vertically above the ground-state IRC points (circles). Bottom: reaction profile with no symmetry restrictions.

sufficiently strong to break the symmetry and may thus well cause the appearance of a second imaginary mode of negative frequency.

Following this mode, which leads to a mixing of the ^{2}A and the ^{2}B wave functions, did indeed lead us to a first-order saddle point, **TS3**, at the B3LYP level, but this turned out to connect **CB**$^{\bullet+}$ to **BCB**$^{\bullet+}$ instead of *trans*-**BD**$^{\bullet+}$, a new reaction pathway that will be discussed in the following section. However, on further exploration of this region of the potential surface, we eventually found another first-order saddle point, **TS2**, at the B3LYP and QCISD levels. IRC calculations (Figure 6 lower panel) demonstrated that this corresponds indeed to the elusive **CB**$^{\bullet+}$ → *trans*-**BD**$^{\bullet+}$ transition state. Interestingly, the structural features of **TS2** are reminiscent of those of the cyclopropylcarbinyl radical cation which had been proposed as an intermediate by Bauld.[11] In particular, the C_1-C_3 distance which is more than 2.1 Å in reactant and product is reduced to 1.89 Å at the B3LYP level (1.74 Å by QCISD), and it shrinks by another 0.14 Å along the B3LYP IRC before increasing again on the way to *trans*-**BD**$^{\bullet+}$.

Despite this surprising departure from the adiabatic C_2 reaction pathway connecting **CB**$^{\bullet+}$ to *trans*-**BD**$^{\bullet+}$, the IRC calculation shows that the conrotatory motion of the CH_2 groups, on which the system engages at the outset, is preserved throughout the reaction. The reason for this is that rotation of the exocyclic CH_2 group is strongly hindered due to hyperconjugative interaction of the empty p-AO on that group with the filled σ-MOs of the three-membered ring.

Thus it appears that there are *two* reaction pathways connecting **CB**$^{\bullet+}$ to **BD**$^{\bullet+}$, both of which are concerted and nonsynchronous, but conrotatory. Comparison of the activation energies and/or 298 K enthalpies for the two processes at the highest level of theory (cf. entries for **TS1** and **TS2** in the last column of Table 3) shows that they lie within 1 kcal/mol, i.e., within the expected accuracy of the method. Moreover, accounting for solvation by the polarizable continuum model (PCM)[38,39] leads to a preferential stablization of **TS2** such that the barrier for the rearrangement leading to *trans*-**BD**$^{\bullet+}$ falls below that for going to *cis*-**BD**$^{\bullet+}$.[40] Thus, the two reactions are clearly competitive, in contrast to the earlier conclusions of Wiest.

On the UMP2 surface we could find no transition state corresponding to **TS2**. Instead we found a very shallow minimum flanked by two transition states which connect it to **CB**$^{\bullet+}$ in one direction and to *cis*-**BD**$^{\bullet+}$ in the other one. We

(38) Cossi, M.; Barone, V.; Cammi, R.; Tomasi, J. *Chem. Phys. Lett.* **1996**, *255*, 327.

(39) For a definition of the cavities used in the computation of solvation energies, see: Barone, V.; Cossi, M.; Tomasi, J. *J. Chem. Phys.* **1997**, *107*, 3210.

will come back to these findings in connection with the discussion of what we call the Bauld plateau in section 3.3 below. However, we note already here that the potential energy surface in this region is quite flat at all levels, an effect which is apparently caused by the strong vibronic interactions between the ground and excited states that prevail in this region.

Considerable effort was spent in exploring the alternative *disrotatory* pathway for the **CB**$^{\bullet+}$ → *trans*-**BD**$^{\bullet+}$ reaction, but no stationary points could be located at any level. On increasing the $C_1-C_2-C_3-C_4$ dihedral angle, starting from **CB**$^{\bullet+}$, unconstrained geometry optimizations invariably resulted in a conrotatory motion of the terminal CH_2 groups, and all attempts to enforce a disrotatory twisting led to an increase of the energy. Thus we are led to conclude that the conrotatory pathway outlined in Figure 6 is indeed the lowest one connecting **CB**$^{\bullet+}$ to *trans*-**BD**$^{\bullet+}$.

3.2.3. *cis*-BD$^{\bullet+}$ → BCB$^{\bullet+}$ Reaction. As mentioned in the previous section we serendipitously located an additional transition state, **TS3**, which was found by IRC calculations to connect *cis*-**BD**$^{\bullet+}$ to the bicyclic **BCB**$^{\bullet+}$ (cf. Figure 7, lower panel). Examination of the frontier orbitals of *cis*-**BD**$^{\bullet+}$ and **BCB**$^{\bullet+}$ indicate that it is a symmetry allowed reaction along a C_2 coordinate, as the ground states of both species connect adiabatically on a ^{2}A surface (Figure 7, upper panel). In striking similarity to the previous case of the **CB**$^{\bullet+}$ → *trans*-**BD**$^{\bullet+}$ reaction, the stationary point which can be located on the C_2 ground-state surface turns out to be a second-order saddle point, **SP2-3**. The pronounced curvature of the potential energy surface at this point indicates that the correlation of the ground state of **BCB**$^{\bullet+}$ is really into a ^{2}A *excited* state of *cis*-**BD**$^{\bullet+}$, and inspection of the FMOs shows this to be one where the unpaired electron resides in the totally antibonding π-MO. It is easy to show that the same is true of the reverse reaction.

More importantly, the true transition state for this process, **TS3**, has no symmetry. This suggests again the intervention of vibronic interaction which may be traced to the proximity of an excited state of opposite symmetry to the ground state. The single-point calculations of the ^{2}B state at the IRC points on the ^{2}A surface shown in Figure 7 indicate, however, that the two states do not get as close as in the previous case (cf. Figure 6). Despite this, vibronic interaction between them is sufficiently strong to depress the activation barrier for the **BCB**$^{\bullet+}$ → *cis*-**BD**$^{\bullet+}$ rearrangement from about 44 kcal/mol on the C_2 surface to about 18 kcal/mol when it proceeds via **TS3** and to a general flattening of the ground-state surface in the vicinity of that transition state. This must be due to a large matrix element for the mixing of the ^{2}A and the ^{2}B state on distortion and/or a very small force constant for the symmetry-breaking normal mode in the ^{2}A state in the absence of vibronic interaction. It shows that, even in symmetry-allowed reactions, symmetrical reaction paths can never be taken for granted in radical ions, despite the absence of an obvious proximity of states of different symmetry.

Although **TS2** and **TS3** have quite distinct geometrical features (see Figure 8), their electronic structure is quite similar. In both, the HOMO (and hence the spin) is localized largely on the slightly pyramidal C−H unit in the three-membered ring whereas the charge is centered mostly on the exocyclic CH_2 group (cf. FMOS in the lower panel of Figure 7). Thus, both can be regarded as cyclopropylcarbinyl radical cations of the type proposed by Bauld. Actually, it is rather surprising that the two above rearrangements occur via transition states of such similar nature because they "originate" from two adiabatic surfaces of opposite symmetry in C_2 (^{2}A for the *cis*-**BD**$^{\bullet+}$ → **BCB**$^{\bullet+}$ and ^{2}B for the **CB**$^{\bullet+}$ → *trans*-**BD**$^{\bullet+}$ rearrangement). The crossing point between these two surfaces which is shown in Figure 9 should really be regarded as the "starting point" for the vibronic interactions which lead to **TS2** and **TS3**.

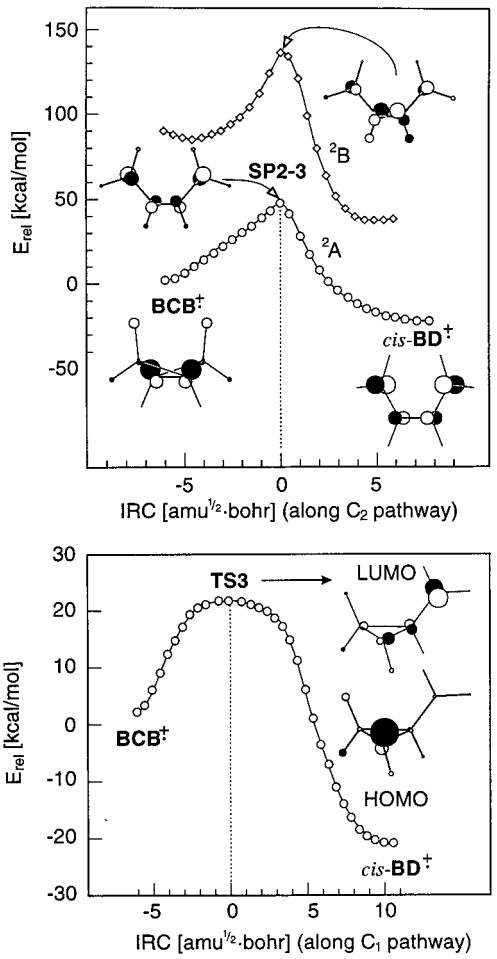

Figure 7. Energy profile for the **BCB**$^{\bullet+}$ → *cis*.**BD**$^{\bullet+}$ ring-opening reaction from B3LYP/6-31G* IRC calculations. Top: reaction profile under maintenance of C_2 symmetry (insets show the singly occupied MO for different states at stationary points on the reaction pathway). The excited-state surface is coposed of points (squares) vertically above the ground-state IRC points (circles). Bottom: reaction profile with no symmetry restrictions (inset shows frontier MOs at the geometry of **TS3**).

3.2.4. Alternate Reaction Paths Connecting the Four $C_4H_6^{\bullet+}$ Isomers. Next to the above reaction pathways we also searched for others which would connect the four $C_4H_6^{\bullet+}$ isomers discussed in this study. First, we found one for the nearly isothermal **BCB**$^{\bullet+}$ → **CB**$^{\bullet+}$ rearrangement which involves a transition state, **TS4**, that corresponds to a hydrogen shift from a CH_2 to a CH group in **BCB**$^{\bullet+}$ (see Figure 8). IRC calculations show that the C_1-C_4 bond, which is actually shorter in **TS4** than in **BCB**$^{\bullet+}$, begins to elongate shortly after the transition state whereupon the system collapses without further activation to **CB**$^{\bullet+}$. At the highest level of theory, **TS4** lies, however, about 14 kcal/mol higher in energy than **TS1**−**TS3** and hence the **BCB**$^{\bullet+}$ → **CB**$^{\bullet+}$ reaction is not competitive with the above rearrangements leading to butadiene cations.

(40) Single-point calculations at the B3LYP/6-31G* level give solvation energies in chloroform of 41.7, 37.7, and 41.1 kcal/mol for **CB**$^{\bullet+}$, **TS1**, and **TS2**, respectively. Adding these to the RCCSD(T) numbers in Table 3 leads to activation enthalpies of 21.4 and18.8 kcal/mol for the rearrangements leading to *cis*- and *trans*-**BD**$^{\bullet+}$, respectively. A more in-depth study on the effect of solvation on the barriers for the two processes, including geometry reoptimizations, is under way (Barone, V.; Rega, N.; Sastry, G. N.; Bally, T. To be published).

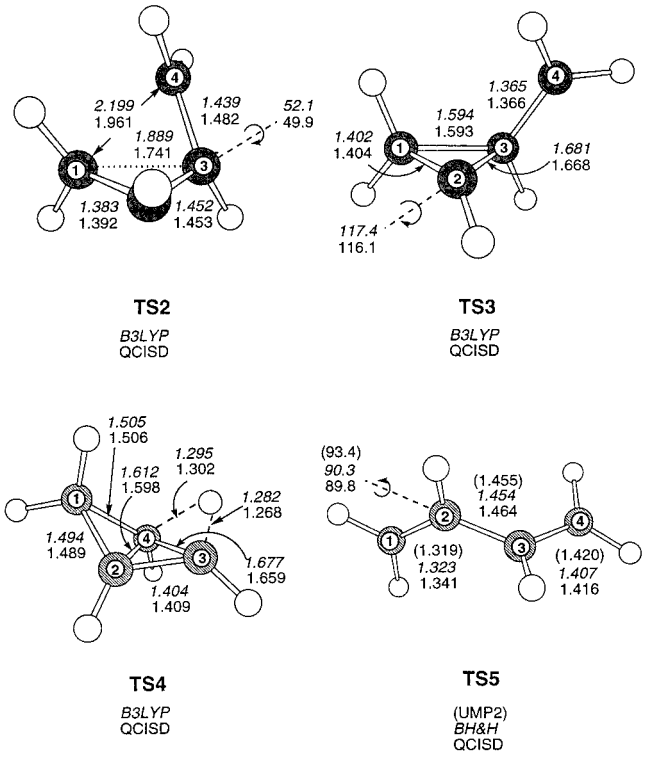

Figure 8. Salient geometrical features of transition states **TS2**−**TS5** as obtained by different methods. Full sets of Cartesian coordinates, energies, and thermal corrections are available in the Supporting Information

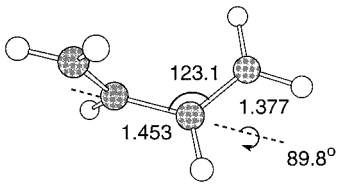

Figure 9. Geometry of the C_2 conical intersection for the crossing of the ^{2}A and the ^{2}B surfaces of $\mathbf{BD}^{\bullet+}$ as obtained by a state-averaged CASSCF calculation.

The direct $\mathbf{BCB}^{\bullet+} \rightarrow$ *trans*-$\mathbf{BD}^{\bullet+}$ rearrangement, analogous to the $2\sigma_s + 2\sigma_a$ process observed for neutral **BCB,**[41] is state symmetry forbidden along a C_2 reaction coordinate in the radical cations. Although the ^{2}A and the ^{2}B surfaces could be traced from reactants to products, all attempts to find a transition state for the adiabatic passage between the two surfaces led to one or the other of the stationary points discussed before. From this we conclude that the $\mathbf{BCB}^{\bullet+} \rightarrow$ *trans*-$\mathbf{BD}^{\bullet+}$ rearrangement must occur in two distinct steps in the radical cation.

Finally, we searched for the transition state for the *cis*- to *trans*-$\mathbf{BD}^{\bullet+}$ isomerization. In contrast to the neutral where this corresponds to rotation around an essential single bond with an activation energy of only 3 kcal/mol (gauche → trans),[42] removal of an electron from the HOMO which is bonding along the central C−C bond results in a considerable increase in the π bond order and therefore also in the rotational barrier. An estimate for the activation barrier can be obtained from the first excitation energy of $\mathbf{BD}^{\bullet+}$ which corresponds to the splitting of the ethylenic π-MOs that is reduced to (nearly) zero at the perpendicular geometry that prevails in the transition state. The $^2A_u \rightarrow {}^2B_g$ excitation energy in $\mathbf{BD}^{\bullet+}$ is nearly 2 eV,[43] so the activation energy should be around 1 eV.

This semiquantitative estimation was eventually confirmed by the calculations which give an activation enthalpy of 22.4 kcal/mol for this process at our highest level of theory. However, locating the transition state, **TS5**, for the *cis*- to *trans*-$\mathbf{BD}^{\bullet+}$ isomerization turned out to be no trivial matter. It can easily be seen that, along a C_2 pathway, the ground state of one rotamer correlates with the first excited state of the other and vice versa, hence the process is state symmetry forbidden in C_2 symmetry. Inspection of the wave functions shows that, to effect passage from the ^{2}A to the ^{2}B surface, the system must localize the HOMO, and hence spin and charge, in one of the double bonds so that the coefficients in the other part can change sign.

As we have shown recently[24] current density functionals cannot correctly model such situations requiring localization of spin and charge, which occur quite frequently in radical ion reactions. This failure makes it impossible to locate certain transition states, unless a significant amount of Hartree−Fock exchange density is admixed, as in Becke's "half-and-half" method. Indeed, we eventually succeeded to locate **TS5** by this method and then to reoptimize it by QCISD, but any attempt to find a corresponding stationary point on the BLYP or B3LYP surfaces proved futile.

TS5 shows the expected features (cf. Figure 8), i.e., a long and a short $CH-CH_2$ bond (1.34 and 1.42 Å, respectively, at QCISD) in a butadiene frame twisted by nearly 90°. Inspection of the FMOs confirms their localization in the longer of the two bonds. It is interesting to note that **TS5** looks very similar to the ^{2}A/^{2}B crossing point shown in Figure 9, apart from the unequal terminal C−C bond lengths. However, this should come as no surprise because there is no reason for the system to depart more from the C_2 crossing point than is necessary to effect the required localization of spin and charge. The energy of **TS5** lies well below that of **TS1**−**TS4**, so any $\mathbf{CB}^{\bullet+}$ that have sufficient energy to decay to $\mathbf{BD}^{\bullet+}$ by one or the other route described above will have sufficient energy to overcome the *cis*- to *trans*-$\mathbf{BD}^{\bullet+}$ barrier, provided that the excess energy is not rapidly dissipated. In condensed phase, where this is the case, $\mathbf{BD}^{\bullet+}$ may well be trapped preferentially in one or the other conformation, depending on what route is followed in the ring-opening process.

3.2.5. Some Methodological Remarks. Table 3 summarizes the relative energies of all the species discussed so far, as obtained by the different methods employed in this study. The DFT and the UQCISD energies were calculated at the geometries that were optimized at the respective levels, whereas the last four columns represent single-point RCCSD(T) calculations with a triple-ζ basis set. Two sets of such calculations were carried out to show how little the results depend on whether they are based on B3LYP or QCISD geometries: the relative energies never differ by more than a kcal/mol, even for transition states, and usually by only a few tenths of that.[44]

However, this does not imply that the geometries obtained by the two methods are identical. At potential energy minima, B3LYP bond lengths are slightly but systematically longer (cf. Figure 2), whereas at transition states, they vary more strongly,

(41) Closs, G. L.; Pfeffer, P. E. *J. Am. Chem. Soc.* **1968**, *90*, 2452.
(42) Murcko, M. A.; Castejon, H.; Wiberg, K. B. *J. Phys. Chem.* **1996**, *100*, 16162.
(43) Bally, T.; Nitsche, S.; Roth, K.; Haselbach, E. *J. Am. Chem. Soc* **1984**, *106*, 3927−3933.
(44) Note that the differences between the entries in the two ΔE_0 columns do not correspond to the differences in total energies. However they come very close because the latter difference amounts to only 0.02 kcal/mol for $\mathbf{CB}^{\bullet+}$ (it is less than 10^{-3} kcal/mol for either $\mathbf{BD}^{\bullet+}$!). Complete listings of total energies are available in the Supporting Information.

especially with regard to C−H or C−C bonds that are being broken and formed (cf. **TS1** in Table 2 and **TS2**−**TS4** in Figure 8). In these cases the RCCSD(T) energies obtained at the QCISD geometries are systematically *lower* than those at the B3LYP geometries, but as we are dealing with transition states, this does not prove the superiority of either method in predicting accurate geometries.

In any event, it is very reassuring to note that it does not seem to matter much if high-level single-point energy calculations are based on QCISD or on the (much more economically obtained) B3LYP geometries, except in cases where DFT runs into the kind of problems discussed in section 3.2.4, in which case it might be altogether impossible to locate a transition state. Also, the thermal corrections to the energies seem to be largely invariant to the choice between the two methods, as the ΔH_{298} entries in the RCCSD(T) columns vary little more than the ΔE_0 entries. This proves the suitability of B3LYP for frequency calculations which has been noted previously in connection with vibrational studies.[45]

With regard to the DFT *energies* listed in Table 3, it is interesting to note a tendency of overstabilization of **BD**$^{\bullet+}$ compared to the other stable $C_4H_6^{\bullet+}$ isomers. The experimental enthalpy difference between **CB**$^{\bullet+}$ and *trans*-**BD**$^{\bullet+}$ of 19.6 ± 1.5 kcal/mol[46−50] is perhaps slightly overestimated by RCCSD(T)/cc-pVTZ (cf. ΔH_{298} entries), so the corresponding ΔE_0 differences should also be taken as an upper limit. Interestingly the overstabilization of *trans*-**BD**$^{\bullet+}$ by the DFT methods, which is quite pronounced with BLYP, decreases with increasing admixture of HF exchange density. Of course, the same discrepancies could also indicate an overestimation of the strain energy of **CB**$^{\bullet+}$, but the DFT energies of **BCB**$^{\bullet+}$ relative to **CB**$^{\bullet+}$—although deviating from those obtained at the reference level—do not exhibit any systematic change on increasing HF exchange density. Thus we conclude that BLYP and, to a lesser degree, B3LYP have a tendency to overstabilize conjugated radical cations relative to unconjugated ones.

Turning to activation barriers (transition state energies), the B3LYP predictions are by far the closest to those obtained at the reference level (average deviation: +4.0 kcal/mol). Admixture of more (BH&H) or less HF exchange density (BLYP) worsens the agreement with the RCCSD(T) results. There is a systematic tendency for a slight overestimation of activation barriers by DFT which is most pronounced for the H-shift reaction leading from **BCB**$^{\bullet+}$ to **CB**$^{\bullet+}$ (**TS5**). However, the predictions of kinetic parameters obtained with the B3LYP procedure represent a vast improvement over those obtained at the UHF, ROHF, or UMP2 levels (cf. energies listed in the Supporting Information). It appears that the best recipe for reliable predictions are B3LYP/6-31G* geometry optimizations followed by RCCSD(T) single-point calculations, preferably with a triple-ζ basis set.

3.3. "Bauld Plateau". As shown above, the IRC plots for the **CB**$^{\bullet+}$ → *trans*-**BD**$^{\bullet+}$ and the *cis*-**BD**$^{\bullet+}$ → **BCB**$^{\bullet+}$ rearrangements are very flat near the corresponding transition states, **TS2** and **TS3**, due to the vibronic interactions which prevail in this region. Transition state searches are very difficult in such flat regions of potential energy surfaces and the nature of the critical points often changes between different levels of theory. Thus, some methods predicted minima (UHF, ROHF, and UMP2), whereas others gave only transition states (DFT and QCISD). However, all of these stationary points (which lie within a few kcal/mol for each method) share certain features, i.e., a three-membered ring containing a spin-bearing CH unit and an exocyclic CH_2 group which carries a good part of the positive charge. These features are representative of the structure that had been proposed by Bauld et al. as an intermediate in the **CB**$^{\bullet+}$ → **BD**$^{\bullet+}$ rearrangement[11] which led us to call the flat region of the potential energy surface that comprises these structures, the "Bauld plateau".

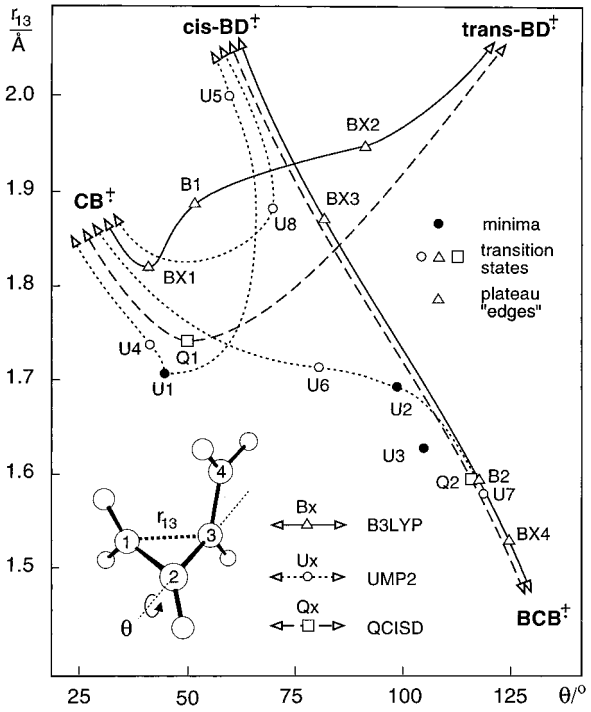

Figure 10. Schematic representation of the different stationary points on the Bauld Plateau as a function of two geometrical parameters. Filled symbols denote minima, open symbols transition states, and hashed triangles BX1-BX4 "edges" of the plateau. Reaction pathways are indicated by lines (solid, B3LYP, dashed, QCISD, dotted, UMP2.

Figure 10 shows the location of all the stationary points found by the UMP2, B3LYP, and UQCISD methods on the "Bauld plateau" as a function of two important structural parameters, the distance r_{13} and the dihedral angle θ, as well as their connection to the stable $C_4H_6^{\bullet+}$ isomers (arrows). Also indicated in Figure 10 (points BX1-BX4) are the points of highest curvature of the B3LYP IRC plots, i.e., the "edges" of the Bauld plateau where the species fall into the exit channels leading to one of the four stable isomers.

Although not identical, the QCISD (dashed lines) and B3LYP pathways (solid lines) are similar as both methods predict only two transition states in this region. In contrast, the UMP2 surface (dotted lines) shows a host of stationary points, not all of which were located because not all minima (solid dots) were connected to transition states (open circles) by IRC calculations. **TS1** (U8 in Figure 10) lies also in the region of the Bauld structures, in contrast to the QCISD and DFT results. U1, another structure with a very small $C_1-C_2-C_3-C_4$ dihedral angle, similar to **TS2** at the QCISD and B3LYP levels (Q1 and B1 in Figure 10), is a flat UMP2 minimum that connects via

(45) Rauhut, G.; Pulay, P. *J. Phys. Chem.* **1995**, *99*, 3093.
(46) From ΔH_f° (**BD**) = 26.0 ± 0.2 kcal/mol,[47] I_a (**BD**) = 9.082± 0.004 eV;[48] ΔH_f° (**CB**) = 37.5 ± 0.4 kcal/mol,[49] and I_a (**BD**) = 9.43 ± 0.02 eV.[50]
(47) Prosen, E. J.; Maron, F. W.; Rossini, R. D. *J. Res. Natl. Bur. Stand.* **1951**, *46*, 106.
(48) Mallard, W. G.; Miller, J. H.; Smyth, K. C. *J. Chem. Phys.* **1983**, *79*, 5900.
(49) Wiberg, K. B.; Fenoglio, R. A. *J. Am. Chem. Soc.* **1968**, *90*, 3395.
(50) Bieri, G.; Burger, F.; Heilbronner, E.; Maier, J. P. *Helv. Chim. Acta* **1977**, *60*, 2213.

two transition states (U4 and U5) to $\mathbf{CB}^{\bullet+}$ on one end and to *cis*-$\mathbf{BD}^{\bullet+}$ at the other.

Thus, UMP2 predicts *two* pathways for this particular interconversion, one direct (via U8), the other stepwise (via U4−U1−U5). Conversely, no direct pathway connecting $\mathbf{CB}^{\bullet+}$ to *trans*-$\mathbf{BD}^{\bullet+}$ could be found at the UMP2 level, but instead, we found one connecting $\mathbf{CB}^{\bullet+}$ to $\mathbf{BCB}^{\bullet+}$ (via U6−U2−U7), which does not exist at B3LYP or QCISD. All of this instills little confidence in the UMP2 method as a structural predictor in such situations. As none of the species U1−U8 in Figure 10 show significant spin contamination, the discrepancies between the UMP2 and the other results must be due to inadequacies in the second-order perturbation method used to recover correlation energy.

It is interesting to ask how and why such a flat region of the potential energy surface as the Bauld plateau can arise. We believe that two reasons are primarily responsible for this: First, bonding in radical ions is generally weaker than in the parent neutral compounds; therefore, radical ions offer less resistance to geometrical deformations, which results in and by itself in flatter potential surfaces. Second, and more importantly, radical ions distinguish themselves by *low-lying excited states* which greatly favor *vibronic interactions*. Whereas these are already prevalent at the equilibrium geometries of radical ions (where they often lead surprising departures from maximal symmetry), they become very important near transition states, where states of different symmetry may cross (as in the $\mathbf{CB}^{\bullet+} \rightarrow$ *cis*-$\mathbf{BD}^{\bullet+}$ rearrangement, cf. Figure 5) or come very close (as in the $\mathbf{CB}^{\bullet+} \rightarrow$ *trans*-$\mathbf{BD}^{\bullet+}$ rearrangement, cf. Figure 6). Vibronic interactions will tend to maximize the gap between the two surfaces[51] which generally entails a flattening of the lower one of them. The tendency of force constants, which oppose deformations induced by vibronic interactions, to be weaker in radical ions (cf. first reason above) reinforces these deformations and lead to a further flattening.

Taken together, these factors lead to a quite general tendency of radical ion rearrangements to avoid steep regions of potential energy surfaces such as they tend to occur along concerted reaction pathways. Thus, even if distortions are not required because the reactant and product surfaces are of different symmetry, i.e., if no principled reasons prevent an adiabatic passage along a symmetric, concerted pathway, departure form that symmetry is possible, and indeed likely to occur, in a radical ion rearrangement. In such situations of flat potential surfaces near transition states, classical kinetics is bound to break down because dynamics take over, as it has been demonstrated for the related case of the cyclopropane stereomutation via a trimethylene biradical.[52,53] Thus, the choice of an exit channel for any molecule that is projected onto the Bauld plateau will depend on the direction from which it came and the momentum with which it was imparted at that time.

4. Conclusions

Figures 11 shows a schematic overview of the processes examined in this study. We have demonstrated that the ring opening of the cyclobutene radical cation ($\mathbf{CB}^{\bullet+}$) may occur along two competing pathways leading to *cis*- and *trans*-butadiene radical cation ($\mathbf{BD}^{\bullet+}$). At the highest level of theory employed in this study, RCCSD(T)/cc-pVTZ//QCISD/6-31G*, the 298 K activation enthalpies for the two processes differ by less than 1 kcal/mol, which is well within the accuracy of this type of calculation. Moreover, preliminary calculations including solvent effects indicate a preference for the $\mathbf{CB}^{\bullet+} \rightarrow$ *trans*-$\mathbf{BD}^{\bullet+}$ process. The computed activation enthalpies for the two reactions (17−18 kcal/mol) stand also in marked contrast to the experimental activation enthalpy of 7 kcal/mol proposed some time ago by Gross et al.[4] This discrepancy is far beyond what is to be expected from the theoretical methods used in this study, which indicates that this number is in need of a reevaluation.

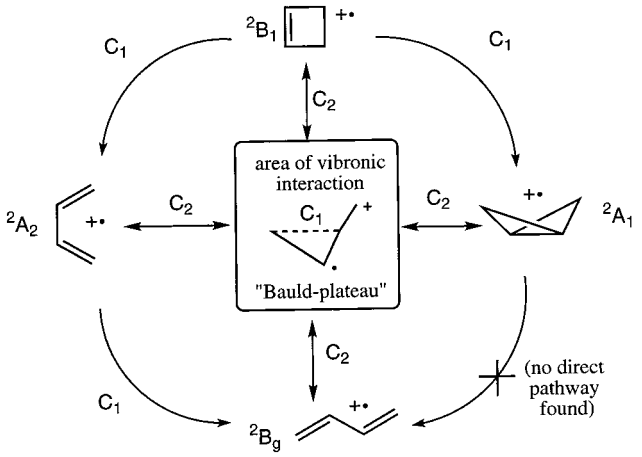

Figure 11. Schematic overview of the processes examined in the present study.

Interestingly, the conrotatory stereochemistry is preserved along *both* pathways, nonwithstanding the fact that the rotation of the CH_2 groups occurs in a highly nonsynchronous fashion. This retention of stereochemistry may explain the experimental finding of controtatory ring opening in subtituted $\mathbf{CB}^{\bullet+}$, even without assuming formation of the less stable cis rotamer.[9] Also, the observation that *trans*-$\mathbf{BD}^{\bullet+}$ is the primary product of photochemical $\mathbf{CB}^{\bullet+}$ ring opening[8] may be explained effortlessly on the basis of the present results, provided that it is regarded as a photochemically activated thermal reaction.

Our search for the transition state for the $\mathbf{CB}^{\bullet+} \rightarrow$ *trans*-$\mathbf{BD}^{\bullet+}$ ring-opening reaction led us into a very flat region of the potential energy surface which comprises structures that resemble the cyclopropylcarbinyl cations that were proposed some time ago as possible intermediates in this process by Bauld et al.[11] It actually turned out that another transition state, i.e., that for the rearrangement of the bicyclobutane radical cation ($\mathbf{BCB}^{\bullet+}$) to *cis*-$\mathbf{BD}^{\bullet+}$, is of a very similar nature. Thus we were able to confirm this prediction of Bauld, although high-level calculations indicate that only transition states, rather than intermediates, correspond to these structures.

Next to the above-mentioned pathways, we also found a transition state for the nearly thermoneutral $\mathbf{BCB}^{\bullet+} \rightarrow \mathbf{CB}^{\bullet+}$ conversion which consists essentially of a 1,2-H shift in concert with a cleavage of the central C−C bond. This process requires, however, much more activation than the $\mathbf{BCB}^{\bullet+} \rightarrow$ *cis*-$\mathbf{BD}^{\bullet+} \rightarrow \mathbf{CB}^{\bullet+}$ sequence and is therefore of little practical relevance. Great difficulties were encountered in the location of the transition state for the *cis*- to *trans*-$\mathbf{BD}^{\bullet+}$ rotamerization by DFT methods. These difficulties can be traced back to the reluctance of DFT methods to separate spin and charge in inherently symmetric radical ions which expresses itself also in an incorrect dissociation behavior of such species.[24] We found that admix-

(51) CASSCF calculations in the region of the Bauld plateau show that the lowest excited state generally lies 50−60 kcal/mol above the ground state, as opposed to less than 20 kcal/mol at some points along the C_2 reaction coordinates (cf. Figures 5−7).

(52) Doubleday: C.; Bolton, K.; Hase, W. L. *J. Am. Chem. Soc.* **1997**, *119*, 5251; *J. Phys. Chem. A* **1998**, *102*, 3648.

(53) Hrovat, D. A.; Fang, S.; Borden, W. T.; Carpenter, B. K. *J. Am. Chem. Soc.* **1997**, *119*, 5253.

ture of enough Hartree−Fock exchange density may remedy the problem and we propose to use Becke's "half-and-half" method in such difficult cases.

Generally, we found that geometries and zero-point energies obtained by gradient corrected DFT models, in particular the hybrid B3LYP method, are so close to those calculated by the much more expensive QCISD method that higher level coupled cluster calculations yield nearly identical energies. This applies equally to transition states whose energies are, however, slightly overestimated by B3LYP, when compared to our reference level of theory. Thus, unless one runs into problems with localization of spin and charge, the B3LYP model appears to be well suited as a starting point for the present kind of study. It will be interesting to see how substitution affects the relative activation energies for the different processes discussed above.

Acknowledgment. This work has been funded through Grant No. 2028-047212.96/1 of the Swiss National Science Foundation and a grant from the Swiss Federal Office for Science and Education in the framework of COST action D3 (Theory and Modeling of Chemical Systems and Processes), of which this joint project between the University of Fribourg (Institute of Physical Chemistry) and the Academy of Sciences of the Czech Republic (Heyrovsky Institute) forms a part. Funding in Prague was provided by the Ministry of Education of the Czech Republic. We thank the Swiss Center for Scientific Computing in Manno for a generous allocation of CPU time on the NEC SX-3/SX4 supercomputer, without which the coupled cluster calculations would have been impossible to carry out. We thank Prof. Wiest for communicating the results of his study to us prior to publication. T.B. gratefully acknowledges enlightening discussions with Profs. Ff. Williams (University of Tennesse) and I. Bersuker (University of Texas) on the subject of vibronic interactions. We are very indebted to Prof. V. Barone (University of Naples), who provided his new PCM code (which will be available in Gaussian 98) to us and instructed us on its use in computing solvation effects. Fianlly, we thank Prof. S. Shaik (Hebrew University) for helpful discussions.

Supporting Information Available: Tables containing the UMP2, B3LYP, and QCISD total energies, thermal corrections, and Cartesian coordinates of all stationary points (minima and transition states) discussed in this study, in ASCII format, are available through the Internet only. See any current masthead page for Web access instructions.

JA981651M